Quantum Electronics **37** (7) 645 – 650 (2007)

INTERACTION OF LASER RADIATION WITH MATTER

PACS numbers: 81.40. – z; 42.62. – b
DOI: 10.1070/QE2007v037n07ABEH013383

Microstructures produced on spatially confined substrates exposed to repetitively pulsed laser radiation

S.I. Dolgaev, N.A. Kirichenko, A.V. Simakin, G.A. Shafeev

Abstract. **The formation of microstructures is studied on metal substrates with characteristic dimensions of tens of micrometers that are comparable with the period of structures produced on extended substrates. Experiments were performed with nickel and nichrome targets composed of wires or a foil. Targets were irradiated in air by 510-nm, 20-ns pulses from a copper vapour laser operating at a pulse repetition rate of 7.5 kHz. Irradiation produced microcones and circular microstructures on substrates. The influence of the target geometry on the morphology and ordering of microstructures formed on it is demonstrated experimentally. The specific features of structures produced on spatially restricted targets are explained by the influence of boundary conditions on their development. A mathematical model of the initial phase of formation of the inhomogeneous profile of the surface of spatially restricted substrates exposed to laser radiation is proposed.**

Keywords: *microstructures, interaction of radiation with matter, metal nanostructures.*

1. Introduction

The formation of microcones under the action of repetitively pulsed laser irradiation has been studied in papers [1 – 5]. The development of microcones was observed in many materials upon laser irradiation of substrates in vacuum and gases. The characteristic period of microcones produced on most of the materials irradiated by nanosecond laser pulses was about 20 μm; this period on steel irradiated by microsecond pulses was 70 μm [6]. In [5], the periodicity of structures formed at initial stages was assigned to capillary waves on the surface of the melt produced upon laser irradiation. It was demonstrated experimentally that the period of microcones depended on the laser pulse duration [7]. We proposed a thermocapillary model of the self-consistent growth of a periodic microrelief [8] and showed the role of the melt flow during the formation stage of structures after the laser pulse end. The authors of [9, 10] demonstrated the localisation and ordering of silicon microcones in the region of interference minima upon Fresnel diffraction of a laser beam from an opaque screen. The localisation of microstructures was explained in [9, 10] by the nonuniform heating of a substrate in the interference light field. The possibility of practical applications of microcones as electron emitters and as the black-body model was demonstrated in papers [11 – 14].

The laser-induced growth of structures has been studied, as a rule, on extended targets of size considerably exceeding the characteristic period of microcones. The dependence of the structure period on the laser beam diameter has not been analysed. At least both for a broad excimer laser beam and a focused beam from a copper vapour laser, the typical period of microstructures was 15 – 20 μm. The formation of structures on spatially restricted substrates such as wires or foils of size comparable with typical periods of microcones was not investigated. Temperature fields produced during pulsed laser heating of such targets can be determined by the substrate geometry and can have its symmetry. The proximity of the substrate edge to the localisation site of structures suggests that the boundary conditions can affect the hydrodynamics of the melt flow, which can influence both the morphology and ordering of microstructures on the target.

2. Experimental

Samples were irradiated by 510-nm, 20-ns pulses emitted by a copper vapour laser with a pulse repetition rate of 7.5 kHz. The laser beam was focused to a spot of diameter ~ 100 μm on the sample surface, providing 5 J cm^{-2} of the radiation energy density in the focal spot. Experiments were performed with nickel, nichrome, and copper targets composed of wires or a foil and also with extended substrates made of the same materials. Targets were made of wires of diameter 50 – 100 μm, which were tightened to circular bundles, and rectangular stacks were made of a 50-μm-thick foil. Target end faces exposed to laser radiation were polished. Samples were irradiated in air by repeatedly scanning the laser beam along the specified path so that each point of the target surface was repeatedly exposed to laser radiation. The number of pulses required for the formation of microcones achieved several thousands. The surface morphology after laser irradiation was studied by using optical or electron microscopy.

S.I. Dolgaev, N.A. Kirichenko, A.V. Simakin, G.A. Shafeev Wave Research Centre, A.M. Prokhorov General Physics Institute, Russian Academy of Sciences, ul. Vavilova 38, 119991 Moscow, Russia; e-mail: kir@kapella.gpi.ru

Received 4 September 2006; revision received 24 January 2007
Kvantovaya Elektronika **37** (7) 645 – 650 (2007)
Translated by M.N. Sapozhnikov

3. Experimental results

Microstructure matrices produced on extended and spatially restricted substrates have different morphologies. Laser irradiation of extended nickel substrates leads to the formation of microcones with period 20 μm on their surface. The apexes of the cones rise above the substrate surface, while their bases are located below its level, which is typical for microcones observed for most of the materials [4, 5]. No ordering of the structures over some directions was observed. Upon laser irradiation of the end faces of a nickel foil, two rows of microcones are formed, which are oriented along boundaries of each of the plates (Fig. 1). At the centre of some plates the third row of cones is formed. The period of microstructures along boundaries of the plates is close to that of nickel microcones on the extended target and is about 20 μm. The distance between the apexes of the cones in the perpendicular direction was 34 μm. The height – base diameter ratio for structures under study achieved 3, which corresponded to the angle of incidence of radiation on the structure surface equal to 72°.

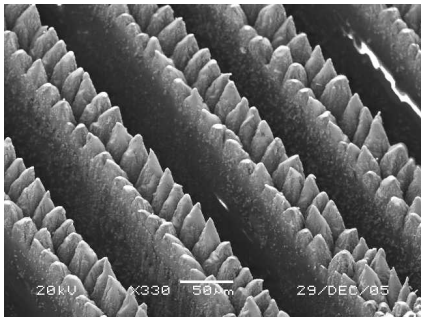

Figure 1. Microcones produced on a nickel foil irradiated by 2×10^3 laser pulses with an energy density of 5 J cm^{-2}. The scale mark is 50 μm.

Upon exposing an extended nichrome substrate to repetitively pulsed laser radiation, microcones with period ~ 25 μm were formed on its surface (Fig. 2a). The surface of structures is covered by an oxide film on which microscopic cracks are observed. On nichrome targets exposed to the same radiation the circular microrelief was formed at the periphery of wires (Fig. 2b). The relief depth on a substrate of diameter 100 μm achieved 30 μm, corresponding to the angle of incidence of radiation on the structure walls equal to 30°. The wire images obtained with an electron microscope exhibit distinct pits localised in the minima of the relief, which are formed due to transfer of the material from the lower parts of the relief to its elevated parts. The number of pits within the site varied from one to several (three or four). The pits were circular, some of then having the triangular cutting. Between the pits the relief elevations oriented in the radial direction were observed. On some wires, the pits were symmetrically located with respect to the substrate axis.

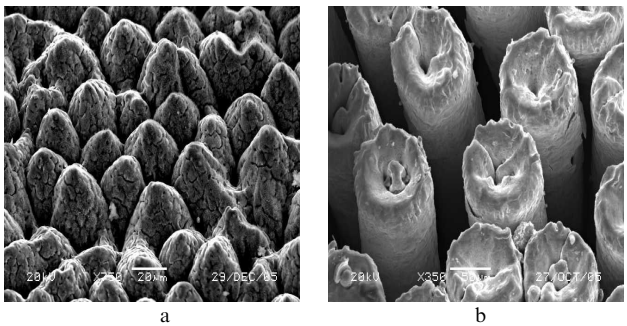

a b

Figure 2. Microreliefs produced on a semi-infinite nichrome plate (a) and nichrome wires (b). The observation conditions are as in Fig. 1. The scale marks are 20 (a) and 50 μm (b).

4. Simulation of the initial stage of the relief formation

The difference of the morphology of structures formed on spatially restricted nickel and nichrome substrates from the morphology of extended substrates can be explained by a considerable influence of boundary conditions. Our experiments show that if a substrate is spatially restricted in one of the directions (Fig. 1), the period of structures can change. A change in the morphology of structures on passing from an extended target (Fig. 2a) to a restricted one (Fig. 2b) is also caused by the spatial restriction of the substrate. In this case, the relief is not periodic: a concave 'cup' is formed on the ends of nichrome wires. In some cases, an elevation is formed at the target centre. The formation of such microstructures can be well described by assuming that they are produced due to the appearance of a thin film of the melt, which begins to flow under the action of capillary and thermocapillary forces. Correspondingly, it is necessary to solve jointly the heat conduction equation and the equation of hydrodynamics of the melt flow in the mathematical model of the process.

We used repetitively pulsed laser radiation in experiments described above. Estimates show that the time interval between laser pulses is so long that the target has time to cool virtually completely after the end of a laser pulse by the onset of the next pulse. This means that the result of the action of a train of pulses preceding a pulse under study is taken into account only by the profile of the target surface produced by them. In this connection we consider a mathematical model describing the action of a single pulse on a spatially restricted target. In this paper, we will restrict ourselves to the case of heating a foil end (corresponding to the microrelief shown in Fig. 1). In addition, we will consider only the initial stage of the process when the curvature of laser-induced structures is small. The latter assumption significantly simplifies the basic equations of the model.

4.1 Heating problem

The first part of the model consists in the description of the target heating and formation of the melt film. We assume that the radiation intensity absorbed by a target is described by the expression

$$I(t) = I_0 \frac{t}{\tau} \exp\left(-\frac{t}{\tau}\right), \tag{1}$$

where τ is the pulse duration. At the initial stage (during several first pulses), the relative deformation of the target surface is small. By assuming in the lowest approximation that the target surface is plane, we can estimate the characteristic thickness of the melt layer and elucidate the

role of evaporation. According to our estimates, the thickness of the melt layer is ~ 1 μm. Because the penetration depth of laser radiation in metals is $\sim 10^{-2}$ μm, we can assume that radiation is mainly absorbed on the metal surface.

The distribution of the temperature field in a target is described by the heat conduction equation

$$c\rho \frac{\partial T}{\partial t} = \frac{\partial}{\partial z}\left(k \frac{\partial T}{\partial z}\right), \quad 0 < z < \infty, \tag{2}$$

where z is the coordinate measured from the target surface deep in the target. At the melting front $z = s(t)$, where s is the melt-layer thickness, the boundary conditions

$$-k \left.\frac{\partial T}{\partial z}\right|_{z=s(t)-0} = -k \left.\frac{\partial T}{\partial z}\right|_{z=s(t)+0} + \rho L_m \frac{ds}{dt},$$
$$T|_{z=s(t)-0} = T|_{z=s(t)+0} = T_m \tag{3}$$

should be fulfilled. Here, the first equality takes into account the solid metal–melt phase transition, and the second one – the continuity of the temperature field and position of the melting front. The quantities c, ρ, k, T_m, and L_m in equations (2) and (3) are the heat capacity, density, heat conductivity, melting point, and specific melting heat of matter, respectively.

For radiation intensities used in our study, evaporation plays a considerable role. The position of the evaporation front is determined by the expression $z = H(t)$, where H is the evaporated layer thickness. Then, the boundary condition on the external surface can be written in the form

$$-k \left.\frac{\partial T}{\partial z}\right|_{z=H} = I - \rho L_v u. \tag{4}$$

The evaporation rate u depends on the surface temperature T_s and is determined by the known expression

$$u(T_s) = u_0(T) \exp\left(\frac{T_v}{T_b} - \frac{T_v}{T_s}\right),$$
$$u_0(T) = \frac{p_0}{\rho T_s}\left(\frac{m T_b}{2\pi k_B}\right)^{1/2}. \tag{5}$$

Here, p_0 is the atmospheric pressure; T_b is the boiling point at the atmospheric pressure; m is the mass of a particle being evaporated (in our case, the mass of a metal atom); k_B is the Boltzmann constant; and the quantity T_v is related to the evaporation heat L_v by the expression $T_v = mL_v \times (\rho k_B)^{-1}$.

The formulated problem was solved numerically and by approximate methods. Let us present some solutions that are substantial for a further discussion. The radiation parameters in (1) were set equal to

$$\tau = 2 \times 10^{-8} \text{ s} \quad \text{and} \quad I_0 = 1.18 \times 10^8 \text{ W cm}^{-2}. \tag{6}$$

We used in calculations the values of parameters typical for nickel:

$$m = 9.63 \times 10^{-23} \text{ g}, \quad \rho L_v = 5.68 \times 10^4 \text{ J cm}^{-3},$$
$$T_b = 3073 \text{ K}, \quad T_m = 1728 \text{ K}, \quad \rho L_m = 2.66 \times 10^3 \text{ J cm}^{-3},$$
$$c = 5.49 \text{ J cm}^{-3} \text{ K}^{-1}, \quad \rho = 8.91 \text{ g cm}^{-3},$$
$$k = 0.66 \text{ W cm}^{-1} \text{ K}^{-1}. \tag{7}$$

To simplify calculations, we assumed that thermal properties of the solid and liquid phases of a metal are the same. Model calculations show that the abandonment of this assumption under our conditions leads to negligible corrections.

Figure 3a shows the time dependence $T_s = T(0, t)$ of the target surface temperature, and Fig. 3b shows the time dependence $s(t)$ of the melt layer width. We found that the width of the evaporated layer under our conditions was

$$H = \int_0^\infty u(T_s(t))dt \approx 0.02 \text{ μm}.$$

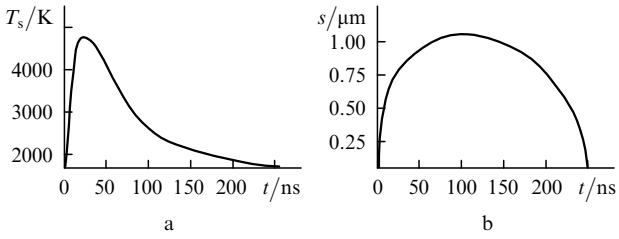

Figure 3. Time dependences of the target surface temperature T_s (a) and the melt layer thickness s (b) upon irradiation by the laser pulse described by relations (1) and (6).

The dependence of the melt layer thickness s on the radiation intensity (during one laser pulse) is also of interest. The solid curve in Fig. 4a shows the maximum melt thickness s_{max} achieved upon the action of a pulse with temporal profile (1) as a function of I_0. For comparison, the dashed curve shows the dependence of the stationary thickness s_{st} of the melt film on the cw radiation of the same intensity I_0.

The dependence $s_{st}(I_0)$ corresponds to the qualitative estimate presented in classical book [15]: $s_{st} \sim s_{max} \sim G/I$, where $G \sim kT_{ev}$, T_{ev} is the characteristic vaporisation temperature, and I is the radiation intensity. This estimate

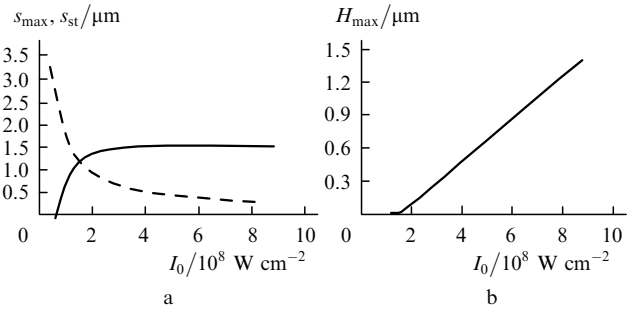

Figure 4. Dependences of the maximum melt thickness s_{max} upon pulsed irradiation (solid curve), the stationary melt thickness s_{st} upon continuous irradiation (dashed curve) (a) and the maximum thickness H_{max} of the evaporated substance layer (b) on the radiation intensity I_0.

reflects the fact that the vaporisation rate drastically increases with increasing the radiation intensity (faster than the velocity of the melting front). This restricts the melt thickness. In the case of pulsed irradiation, melting also occurs when the radiation intensity strongly decreases: the vaporisation rate is no longer small, but the surface temperature is high enough for the melting front to move inside the target.

To emphasise a competition between evaporation and melting, we considered the model problem of the target heating by radiation with a rectangular temporal intensity profile shown in Fig. 5a. Figure 5b shows the corresponding time dependence of the melt thickness. Note that the melt thickness drastically increases at the pulse end.

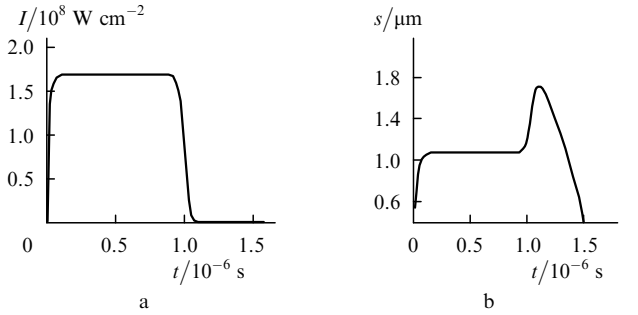

Figure 5. Rectangular time profile of the radiation intensity (a) and the corresponding time dependence of the melt layer thickness (b).

Figure 4b shows the maximal thickness of a matter layer evaporated during a pulse as a function of the radiation intensity I_0 [for the invariable pulse duration τ in (1)].

One can see from Fig. 4a that the melt thickness changes weakly in a broad intensity range. It seems that this is an important factor resulting in a certain versatility of the parameters (amplitude and period) of structures produced by using different lasers and targets.

4.2 Melt flow

Consider now the melt-flow dynamics on a surface. We restrict ourselves to the case of heating a thin metal plate, assuming that the coordinate x is measured along the target surface of width L ($L/2 < x < L/2$) and the coordinate z is measured along the normal to the surface. Irradiation produces a $\sim$ 1-mm-thick melt film on the target surface. By assuming that the melt is an incompressible liquid, we write the equation determining the film thickness:

$$\frac{\partial h}{\partial t} = u_0(x,t) - \frac{\partial (vh)}{\partial x}, \tag{8}$$

where $v = v(x,t)$ is the flow velocity along the surface averaged over the melt cross section; $u_0(x,t)$ is the rate of changing the film thickness caused by melting and cooling. The velocity v can be obtained from the Navier–Stokes equation in the thin-film approximation for a viscous liquid:

$$\eta v = -\frac{1}{3} h^2 \frac{\partial p}{\partial x} + \frac{1}{2} h \frac{\partial \alpha}{\partial x}. \tag{9}$$

Here, η is the melt viscosity, and the pressure

$$p = p_v - \alpha \frac{\partial^2 h}{\partial x^2} \tag{10}$$

in liquid is the sum of the external pressure (vapour pressure) p_v and capillary pressure caused by the surface tension with the coefficient $\alpha = \alpha(T_s)$ depending on the surface temperature T_s. The second term in the right-hand side of (9) takes into account thermocapillary forces appearing due to the inhomogeneity of the temperature field along the liquid surface. We can assume with sufficient accuracy that $\alpha(T) = \alpha_0 + \alpha_1(T - T_{in})$ in a broad temperature range, where α_0 and α_1 are constants and T_{in} is the temperature at which $\alpha(T_{in}) = \alpha_0$. Correspondingly, we have $\partial\alpha/\partial x = \alpha_1(\partial T_s/\partial x)$ in (9). The finite thickness of the target is taken into account by the boundary conditions at the target edges, assuming that $v = 0$ and $h = 0$ for $x = \pm L/2$.

To construct the self-consistent problem of the target heating and melt flow, it is necessary to take into account a change in temperature along the surface. During irradiation, the heat is transferred over the distance $\sim(a\tau)^{1/2} \sim 1$ μm (where a is the thermal diffusivity), which is significantly smaller than the characteristic inhomogeneity scale of the melt along the surface. Under these conditions, the temperature field on the surface virtually reproduces the profile of the source acting on the boundary. Due to deformation, the normal to the surface makes the angle $\varphi(x)$ with the z axis, where $\cos\varphi = [1 + (\partial h/\partial x)^2]^{-1/2}$. It is known that in the case of nonpolarised radiation, the angular dependence of the absorptivity A of metals is described by the expression

$$A(\varphi) = \frac{1}{2} A_0(\cos\varphi + \cos^{-1}\varphi),$$

where A_0 is the absorptivity for normal incidence. Thus, for small deformations of the surface, the local radiation intensity absorbed by matter is

$$I_{abs}(\varphi) = A(\varphi) I_0 \cos\varphi = \frac{1}{2} A_0 I_0 (1 + \cos^2\varphi)$$

$$\approx A_0 I_0 \left[1 - \frac{1}{2}\left(\frac{\partial h}{\partial x}\right)^2\right]. \tag{11}$$

Let us represent the temperature field in matter as the sum

$$T(x,z,t) = T_0(z,t) + \Delta T(x,z,t), \tag{12}$$

where the first term corresponds to the case of a plane surface, and the second term, taking the relief modulation into account, can be written in the form

$$\Delta T(x,z,t) = -\frac{1}{2}\left(\frac{\partial h}{\partial x}\right)^2 F(z,t). \tag{13}$$

The function $F(z,t)$ satisfies the boundary value problem

$$c\rho \frac{\partial F}{\partial t} - \frac{\partial}{\partial z}\left(k \frac{\partial F}{\partial z}\right) = 0, \quad 0 < z < \infty,$$

$$-k \left.\frac{\partial F}{\partial z}\right|_{z=0} = AI - \rho L_v \left.\frac{du}{dT}\right|_{T=T_0} F. \tag{14}$$

The further analysis is based on Eqns (8)–(14), taking into account the dependence $T_0(z, t)$ studied above. The results of the action of a train of pulses can be found by summing deformations produced by individual pulses. The initial conditions for the $n+1$th pulse (the initial surface profile) are determined by the result of the action of the nth pulse.

By using this model, we performed numerical calculations. The target width was set equal to 50 μm. Figure 6 shows the surface profiles produced by the first and second laser pulses.

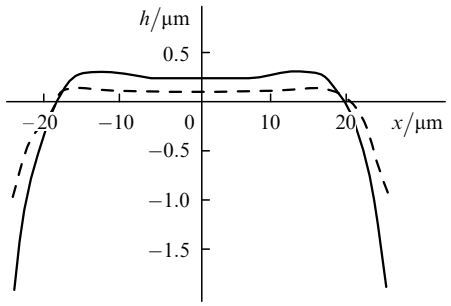

Figure 6. Profiles of the target surface produced after the action of the first (dashed curve) and second (solid curve) laser pulses.

If the initial surface of the target is flat, a 'cup' (a profile with a dip near its centre) is formed already after the first pulse. This effect is caused by a high capillary pressure appearing near the target edges at the initial stage of the structure development. The melt moves from the edges of the target to its centre and from the inner regions to periphery. Calculations show that the melt flow velocity with the target achieves 200 cm s^{-1}. Figure 7 presents the distribution of the flow velocity over the target surface at the instant when the melt thickness is maximal. The velocity $v > 0$ corresponds to the flow in the positive direction of the x axis and $v < 0$ – in the negative direction. The melt flow velocity near the target edges proves to be significant, whereas near the centre the melt is almost at rest. As a result, a 'roller' is formed along the target perimeter, which is 'frozen' after target cooling, thereby fixing variations in the relief. For the same reason, a small local maximum appears on the surface near the target centre. Note that variations of the surface profile from pulse to pulse are relatively small – about 0.1 μm. However, because the same region of the surface is irradiated by hundreds of pulses, the resulting deformation of the surface can achieve several tens of micrometres.

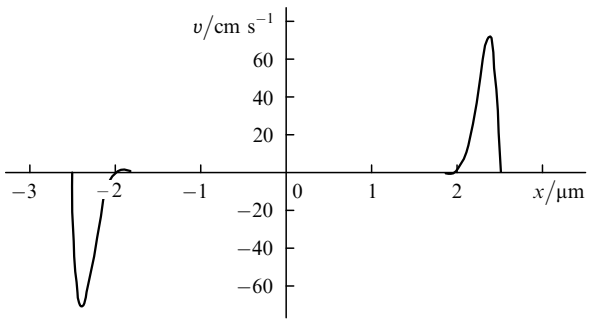

Figure 7. Distribution of the melt flow velocities v over the target surface at the instant $t \approx 1.02 \times 10^{-7}$ s, when the melt thickness is maximal.

It follows from our calculations that capillary and thermocapillary forces make comparable contributions to the mass transfer. However, the temperature gradients along the target surface increase with increasing the surface curvature (in particular, due to a change in the faction of absorbed radiation). As a result, the relative role of the thermocapillary deformation mechanism increases. Calculations showed that upon the action of the first pulses, the vapour pressure does not cause a considerable deformation of the surface because pressure gradients and the characteristic interaction time prove to be small, although the absolute value of the pressure can be considerable (up to 70 atm under our conditions).

The quantitative discussion of the later stages of the surface evolution within the framework of the model proposed above is complicated. However, we can point out qualitatively new mechanisms coming into play. In particular, when the profile slope becomes large, radiation begins to experience multiple reflections from surface inhomogeneities to other regions of the surface.

Irradiation produces cavities at the wire ends at the central part of the substrate, with pits localised at the bottom of cavities (Fig. 2). Note in this connection that the flat surface of the substrate is unstable during its multipulse laser-induced melting and evaporation: a small displacement of the surface deep in the target due to the melt transfer from the centre of the target to its edges produced by one pulse is enhanced under the action of the next pulse. The positive feedback for the instability development is provided by the angular dependence of the absorbed radiation intensity and, hence, the enhancement of bottom heating with increasing the relief depth from pulse to pulse. In this case, the caustic is localised at the substrate centre, providing the primary heating and decrease in the surface tension of the melt and its evaporation at the substrate centre. Under the action of the surface tension gradient, the melt flows in the radial direction from the centre of the substrate to its periphery, increasing the relief depth. The concentration of reflected beams in the relief depressions can produce heating and melting of the material, which can be followed by its intense evaporation. In these regions, the dagger melting mechanism can be realised in which the bending of the surface and removal of the liquid melt due the pressure of the recoil vapours become substantial [15, 16]. In this case, cavities produced in the target have a large depth-to-diameter ratio (more than 1), which is typical for the dagger melting mechanism [16]. We can assume that the regularity in the location of cavities is explained by the symmetry of thermocapillary flows within the circular substrate.

5. Conclusions

We have studied experimentally the formation of microstructures on substrates of transverse size of the order of tens of micrometers exposed to repetitively pulsed laser radiation. The morphology of structures produced on spatially restricted substrates differs considerably from that for extended substrates. The target geometry affects the ordering of the microrelief produced upon irradiation. The formation of structures on spatially restricted sub-

strates is related to the influence of the boundary conditions on the melt flow dynamics. The model of the development of structures on spatially restricted substrates has been proposed which takes into account the heating, melting, and evaporation of the material, as well as its flow under the action of capillary and thermocapillary forces. Simulations have shown that the movement of the material on the surface of a spatially restricted substrate from the centre to periphery is caused by thermocapillary forces, while the reverse flow of the melt from the periphery to centre is caused by the gradient of the capillary pressure. The competition of these processes leads to the formation of a relief with a dip at the centre and maxima at the target periphery.

References

1. Sánchez F., Morenza J.L., Aguiar R., Delgado J.C., Varel M. *Appl. Phys. Lett*., **69**, 620 (1996).
2. Her T.H., Finlay R.F., Wu C., Deliwala S., Mazur E. *Appl. Phys. Lett*., **73**, 1673 (1998).
3. Pedraza A.J., Fowlkes J.D., Lowndes D.H. *Appl. Phys. Lett*., **74**, 2322 (1999).
4. Voronov V.V., Dolgaev S.I., Lavrishchev S.V., Lyalin A.A., Simakin A.V., Shafeev G.A. *Kvantovaya Elektron*., **30**, 710 (2000) [*Quantum Electron*., **30**, 710 (2000)].
5. Dolgaev S.I., Lavrischev S.V., Lyalin A.A., Simakin A.V., Voronov V.V., Shafeev G.A. *Appl. Phys. A*, **73**, 177 (2001).
6. Dolgaev S.I., Fernandez-Pradas J.M., Morenza J.L., Serra P., Shafeev G.A. *Appl. Phys. A*, **83**, 417 (2006).
7. Skantzakis M., Zorba V., Papazoglou D.G., Zergioti I., Fotakis C. *Appl. Surf. Sci*. **252**, 4462 (2006).
8. Dolgaev S.I., Kirichenko N.A., Simakin A.V., Shafeev G.A. *Kvantovaya Elektron*., **34**, 771 (2004) [*Quantum Electron*., **34**, 771 (2004)].
9. Riedel D., Hernandez-Pozos J.L., Palmer R.E., Kolasinski K.W. *Appl. Phys. A*, **78**, 381 (2004).
10. Shen M.Y., Crouch C.H., Carey J.E., Younkin R., Mazur E., Sheehy M., Friend C.M. *Appl. Phys. Lett*., **82** (11), 1715 (2003).
11. Karabutov A.V., Frolov V.D., Loubnin E.N., Simakin A.V., Shafeev G.A. *Appl. Phys. A*, **76**, 413 (2003).
12. Karabutov A.V., Frolov V.D., Simakin A.V., Shafeev G.A. *J. Vac. Sci. Techn. B*, **21**, 449 (2003).
13. Zorba V., Alexandrou I., Zergioti I., Manousaki A., Ducati C., Neumeister A., Fotakis C., Amaratunga G.A.J. *Thin Solid Films*, **453-454**, 492 (2004).
14. Starikov D., Boney C., Pillai R., Bensaoula A., Shafeev G.A., Simakin A.V. *Infr. Phys. Techn*., **45**, 159 (2004).
15. Ready J.F. *Effects of High-Power Laser Radiation* (New York – London: Acad. Press, 1971).
16. Bunkin F.V., Tribel'skii M.I. *Usp. Fiz. Nauk*, **139**, 2 (1980); Tribel'skii M.I. *Kvantovaya Elektron*., **5**, 804 (1978) [*Sov. J. Quantum Electron*., **8**, 462 (1978)].